Reactive and Functional Polymers 216 (2025) 106452

Contents lists available at ScienceDirect

Reactive and Functional Polymers

journal homepage: www.elsevier.com/locate/react

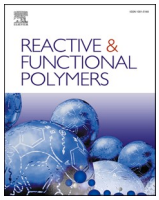

Hybrid polyurethane acrylate films via thiol–ene click and sol–gel reactions: Monomer-dependent structure–property relationships

Bilge Eren [a,*], Sibel Taşpınar [a], Rabia Balci [a], Beyhan Erdoğan [b]

[a] Department of Chemistry, Faculty of Science, Bilecik Seyh Edebali University, 11100 Bilecik, Turkey
[b] DYO Paint Factory, Ataturk Organize Sanayi, Bolgesi, TR-35620 Cigli, Izmir, Turkey

ARTICLE INFO

Keywords:
Hybrid polyurethane acrylate
Sol–gel process
Thermal stability
Crosslink density
Silica network

ABSTRACT

This study introduces a novel strategy for enhancing UV-curable polyurethane acrylate (PUA) coatings by integrating thiol–ene click chemistry with sol–gel processing. Hybrid polyurethane acrylate (HPUA) films were synthesized using biuret-type hexamethylene diisocyanate (HDI) and a pentaerythritol (PENTA) core, followed by end-capping with three structurally distinct acrylate monomers: 2-hydroxyethyl methacrylate (HEMA), 2-hydroxyethyl acrylate (HEA), and 2-hydroxypropyl methacrylate (HPMA). Subsequently, (3-mercaptopropyl) trimethoxysilane (MPTMS) was grafted onto the acrylate-terminated polymers via a thiol–ene click reaction under UV irradiation to introduce alkoxysilane groups for sol–gel hybridization. The objective was to investigate how monomer architecture influences the development of organic–inorganic networks and the resulting thermal, mechanical, and surface properties. FTIR spectral deconvolution confirmed enhanced hydrogen bonding and crosslinking, especially in HPMA-based systems. DSC and TGA results showed that HPMA–HPUA exhibited the highest glass transition temperature (T_g from −13.52 °C to 90.0 °C) and thermal stability (T_{50} from 380 °C to 457 °C), attributed to improved interfacial compatibility with the silica network. Surface analyses revealed increased hardness and hydrophobicity after sol–gel modification, with contact angles rising up to 130°. This study establishes a clear structure–property relationship framework for monomer-dependent hybridization and presents a scalable approach for designing high-performance, UV-curable coatings with customizable thermal and mechanical properties.

1. Introduction

Pentaerythritol (PENTA), a tetrafunctional alcohol, is widely utilized as a crosslinking agent in polyurethane (PU) and hyperbranched polymer (HBP) systems due to its ability to introduce multidirectional branching points. Unlike trifunctional polyols such as glycerol, PENTA facilitates lateral network formation along polymer backbones, enhancing mechanical strength, shape memory, and functional versatility—features particularly beneficial for UV-curable systems.

Numerous studies have highlighted PENTA's structural advantages. Brannigan et al. synthesized thermoplastic polyester urethanes with PENTA-based norbornene groups for post-polymerization functionality and tunable mechanics [1]. Chen et al. reported enhanced acid resistance and thermal stability in PENTA-containing block copolyurethanes [2], while Cho et al. achieved superior shape recovery and tensile strength in shape-memory PUs via PENTA-mediated networks [3]. Similarly, Chung et al. demonstrated increased crosslink density and mechanical performance in PUs incorporating PENTA and PEG-200 spacers [4]. In bio-based polymers, PENTA has enabled improvements in thermal stability and biodegradability, as shown by Das et al. [5], and Lu et al. used PENTA to synthesize compact, thermally stable PU microcapsules [6].

In the coatings field, PENTA-based systems have shown superior performance. For instance, Patel et al. developed fatty acid-modified PU dispersions with enhanced resistance to water and chemicals [7], while Tang et al. synthesized fire-retardant coatings with improved surface and thermal properties [8]. In biomedical contexts, star-shaped amphiphilic PU micelles synthesized from PENTA cores exhibited stable architecture and sustained drug release [9].

Despite these advancements, conventional HBP systems often suffer from brittleness due to dense functional packing and limited chain entanglement, resulting in low elongation at break in UV-cured films. To overcome this, thiol–ene click chemistry has emerged as a powerful strategy for generating uniform, flexible, and oxygen-insensitive

* Corresponding author.
E-mail address: bilge.eren@bilecik.edu.tr (B. Eren).

https://doi.org/10.1016/j.reactfunctpolym.2025.106452
Received 8 May 2025; Received in revised form 6 August 2025; Accepted 13 August 2025
Available online 22 August 2025

crosslinked networks. Wei et al. used castor oil-based HBPU with PETMP to improve flexibility and UV-curing efficiency [10], and similar benefits were reported by Tasić, Džunuzović, Zhang, and Fu in various HBPUA formulations [11–15].

Recent innovations also integrate thiol–ene strategies with PU-based systems for sustainable, high-performance coatings. For example, Xu and Shi demonstrated tunable photopolymerization in HBPUAs modified with succinic anhydride [16], and Xiang, Hu, and Han extended these designs to nanocomposites and photoresists with enhanced mechanical integrity [17–19]. Applications further span optoelectronics and elastomers, where thiol–ene reactions afford high strength and reprocessability [20–23]. Inorganic–organic hybridization via MPTMS, as reported by Ding et al. and Liang et al., further elevates hydrophobicity and thermal durability in polyurethane matrices [24,25].

Building on this foundation, the present work aims to develop UV-curable hybrid polyurethane acrylates (HPUAs) based on PENTA as the multifunctional core and biuret–HDI as the isocyanate source. Three different acrylate monomers—hydroxyethyl methacrylate (HEMA), hydroxyethyl acrylate (HEA), and hydroxypropyl methacrylate (HPMA)—were systematically investigated to elucidate structure–property relationships in the resulting networks. To improve the physical properties of the synthesized systems, a dual-modification strategy was applied: (i) a thiol–ene click reaction, in which (3-mercaptopropyl)trimethoxysilane (MPTMS) was covalently grafted onto the acrylate end groups via UV-induced coupling, and (ii) a subsequent sol–gel reaction, where hydrolyzed alkoxysilane groups underwent condensation to form inorganic Si–O–Si domains uniformly distributed within the polymer network. This hybrid design is expected to improve crosslinking efficiency, thermal resistance, surface hydrophobicity, and mechanical integrity. The resulting materials were thoroughly characterized using FTIR spectroscopy (including carbonyl deconvolution for urethane/urea linkages), DSC, TGA, contact angle analysis, pencil hardness, chemical resistance testing, and SEM imaging of surface and fracture morphology. Overall, this study presents a scalable and effective strategy for the development of UV-curable coatings with adjustable and enhanced thermal and mechanical properties, achieved through the combined methods of thiol–ene click chemistry and sol–gel hybrid network formation.

2. Experimental

2.1. Materials

The materials utilized in this study were procured from various commercial sources. Pentaerythritol (PENTA) was obtained from BASF (Ludwigshafen, Germany), while hexamethylene diisocyanate biuret (HDI-biuret), dibutyltin dilaurate (DBTDL), and the photoinitiator Darocure were supplied by DYO Paints (İzmir, Turkey). Acrylate monomers, including 2-hydroxyethyl methacrylate (HEMA), 2-hydroxyethyl acrylate (HEA), 2-hydroxypropyl methacrylate (HPMA), and (3-mercaptopropyl)trimethoxysilane (MPTMS), were purchased from Sigma-Aldrich. All reagents were used as received, without further purification.

2.2. Characterization

The thermal properties of the polyurethane acrylate films were evaluated using TGA with the EXSTAR SII 7200 instrument (Tokyo, Japan). The samples were heated from 30 °C to 1000 °C at a rate of 10 °C/min under nitrogen atmosphere. The glass transition temperature (T_g) was determined using the Perkin Elmer DSC 6000 differential scanning calorimeter (Norwalk, CT, USA) under a nitrogen atmosphere. A temperature range of −50 °C to 150 °C with a heating rate of 10 °C/min was used. Fourier-transform infrared (FTIR) spectroscopy, performed with the Perkin-Elmer Spectrum-100 instrument (Norwalk, CT, USA), was employed to identify the functional groups present in the samples. The gloss of the PUA films was measured at angles of 20°, 60°, and 85° using a Byk Micro TRI Gloss meter (Silver Spring, MD, USA). Contact angle measurements were performed using an Attension Theta Lite (KSV Instruments, Finland), in combination with a Hamilton Syringe 1001 TPLT. The surface morphology of the PUA films was analyzed using a ZEISS Supra 40 VP scanning electron microscope (Oberkochen, Germany).

2.3. Synthesis of hybrid thiol-ene-polyurethane acrylate polymer (HPUA)

The synthesis of hybrid thiol-ene-polyurethane acrylate polymer (HPUA) was carried out in a three-step process.

Step 1: Pentaerythritol (PENTA) (0.2362 g, 1.7 mmol) was dissolved in 5 mL of acetone and transferred to a reaction flask. In a separate dropping funnel, hexamethylene diisocyanate biuret (HDI-biuret) (3.0 g) was dissolved in 5 mL of acetone and added dropwise to the PENTA solution over the course of 1 h to react with the hydroxyl groups on the PENTA molecule. The reaction mixture was then stirred under a reflux condenser at 45 °C for 2 h.

Step 2: A hydroxy-functional acrylic monomer HEMA (0.9258 g, 6.9 mmol), HEA (0.8434 g, 6.9 mmol), or HPMA (1.0151 g, 6.9 mmol)) was dissolved in 5 mL of acetone and added dropwise to the reaction mixture over 1 h. To catalyze the reaction, 1 mL of dibutyltin dilaurate (DBTL) was added. The mixture was then stirred under reflux at 45 °C for 10 h. The completion of the reaction was confirmed by the disappearance of the isocyanate (NCO) group in the FT-IR spectrum.

Step 3: Upon cooling the reaction mixture to ambient temperature, MPTMS (1.4263 g, 6.9 mmol) was added, followed by Darocure 1173 (0.177 g, corresponding to 3 wt% of the total monomer mass) as the photoinitiator. The mixture was stirred for an additional 2 h under a nitrogen atmosphere to facilitate the thiol–ene photo-click reaction.

To prepare UV-curable films, the MPTMS-modified HPUA solution was coated onto transparent polycarbonate/glass substrates to achieve a film thickness of 50 ± 5 μm. The coated films were then exposed to UVA light (λ = 365 nm, 2 W) at a fixed distance of 2 cm, with a total curing time of 300 s, prior to further characterization.

2.4. Preparation of sol–gel modified HPUA (SHPUA) films

The synthesis of hybrid thiol–ene–polyurethane acrylate polymers was modified through a sol–gel reaction involving MPTMS. To intentionally control the extent of silane condensation and avoid uncontrolled gelation, the reaction was carried out using a weakly basic catalyst (0.1 M NH_3) and limited water content, maintaining a molar ratio of H_2O/Si–OEt = 1. These conditions were selected based on prior studies showing that such parameters favor the formation of partially condensed siloxane networks (T_1–T_2 species) rather than fully crosslinked silica gels [26].

This strategy enables sufficient hydrolysis to initiate silanol (Si–OH) formation and subsequent condensation into Si–O–Si linkages, while maintaining fluidity and avoiding phase separation or premature vitrification. The reaction mixture was gently stirred for 2 h to allow hydrolysis and condensation.

2.5. Gel content measurement

The gel content of both unmodified HPUA and sol–gel modified SHPUA films was determined to evaluate the degree of chemical crosslinking. Rectangular film samples (approximately 1 × 2 cm^2) were first weighed to obtain the initial dry mass (m_1). Each sample was then placed in a Soxhlet apparatus and extracted with acetone for 48 h to remove unreacted monomers, oligomers, and any soluble fractions.

The gel content of the cured films was used to assess the degree of chemical crosslinking. Prior to solvent extraction, the initial dry weight of each UV-cured film sample was recorded as m_1. The samples were then immersed in acetone for 48 h to dissolve unreacted and soluble fractions. Following extraction, the films were dried in a vacuum oven at

30 °C for 72 h until a constant weight was achieved (m_2). The gel content was calculated using the following equation:

$$Gel\ content\ (\%) = \frac{m_2}{m_1} \times 100 \quad (1)$$

All films, including those modified with silane groups (SHPUAs), were subjected to identical UV-curing conditions. Each gel content measurement was conducted in triplicate, and the average value was reported.

3. Results and discussion

3.1. FTIR spectral analysis

FTIR spectroscopy was employed to investigate chemical and structural changes in HEMA-, HEA-, and HPMA-based polyurethane acrylate films before and after sol–gel modification (Fig. 1). In the N—H stretching region (3300–3400 cm^{-1}), distinct shifts were observed depending on the acrylate monomer type (Table 1). For the HEMA-based PUA, the N—H band shifted from 3348.45 cm^{-1} to 3362.10 cm^{-1} after sol–gel treatment, indicating a slight decrease in hydrogen bonding. This change may result from steric hindrance or limited accessibility of N—H groups due to the formation of a siloxane network. A similar, but smaller blue shift was seen in the HEA-based PUA, where the band moved from

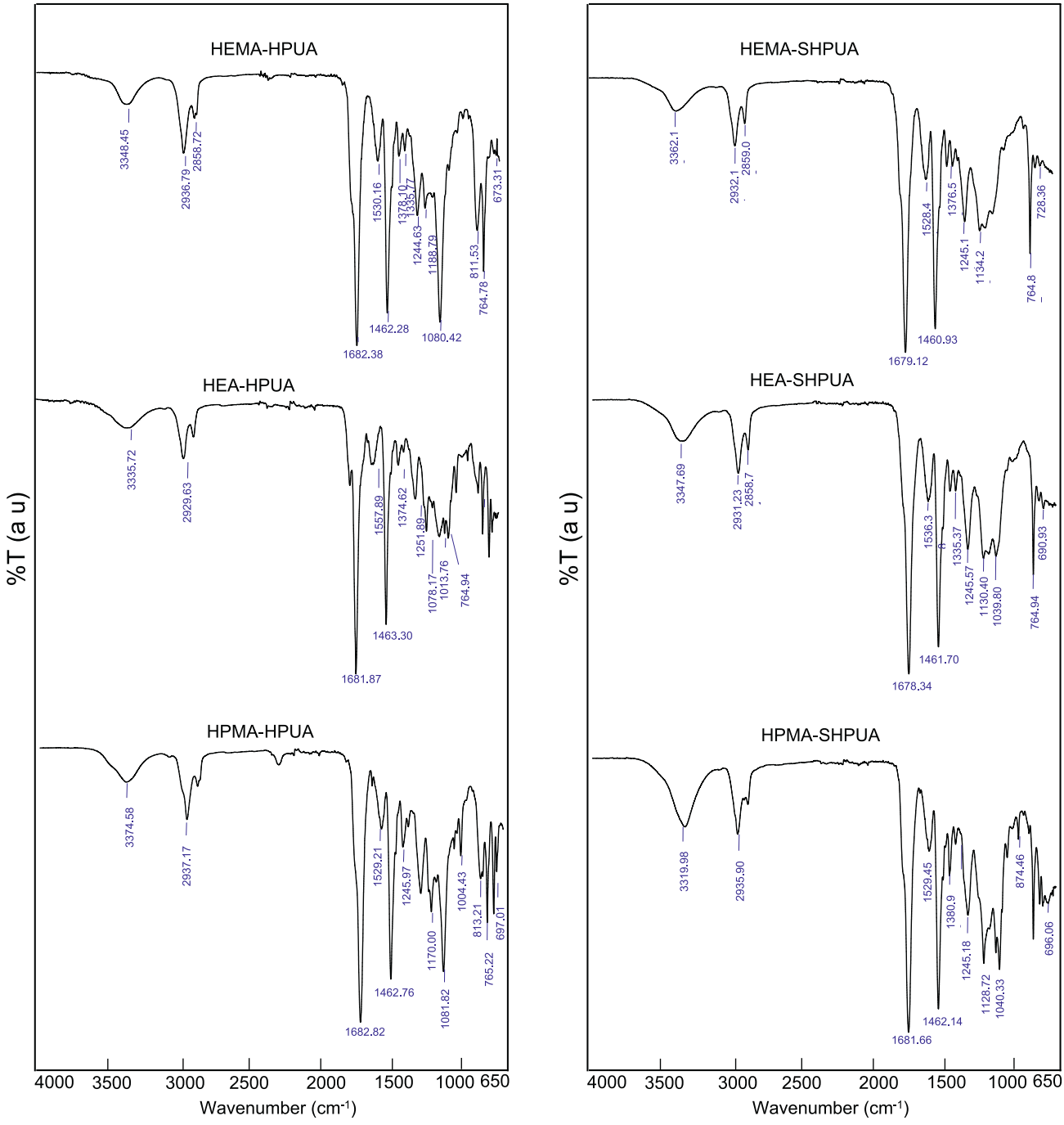

Fig. 1. FTIR spectra of HPUA and SHPUA polymers synthesized with HEMA, HEA, and HPMA monomers.

Table 1
FTIR characteristic band assignments for HEMA-, HEA-, and HPMA-based HPUA and SHPUA polymers.

Assignments[a]	HEMA- HPUA	HEMA- SHPUA	HEA- HPUA	HEA- SHPUA	HPMA- HPUA	HPMA- SHPUA
υ(N—H)	3348.45	3362.10	3335.72	3347.69	3374.68	3319.98
υ_{as}(C—H)	2936.79	2932.11	2929.63	2931.23	2937.17	2935.90
υ_{s} (C—H)	2858.72	2859.06		2858.71	2272.26	
υ(C=O)	1682.38	1679.12	1681.87	1678.34	1682.82	1681.66
Amide II	1530.16	1528.44		1536.38	1529.21	1529.45
δ(CH_3)	1378.10	1376.53	1374.65	1377.17	1375.68	1380.90
υ(C—N)	1355.77	1334.52		1335.37		1335.87
υ(C–O–C)	1244.63	1245.52	1251.89	1245.57	1245.97	1245.18
υ(Si–O–Si)	1188.78	1134.29	1171.43	1130.40	1170.00	1040.33
δ(Si—O)	764.78	764.8	764.94	764.94	765.22	765.18

[a] υ = stretching, as = asymmetric, s = symmetric, δ = bending, ω = wagging, r = rocking.

3335.72 cm^{-1} to 3347.69 cm^{-1}. This also suggests reduced hydrogen bonding, possibly influenced by the flexible ethyl side chain in HEA, which may prevent close packing of functional groups. In contrast, the HPMA-based PUA exhibited a red shift from 3374.68 cm^{-1} to 3319.98 cm^{-1}, indicating an increase in hydrogen bonding, likely due to enhanced structural organization during network formation [27].

In the C═O stretching region, all three formulations showed red shifts following sol–gel treatment, reflecting changes in microstructure and increased hydrogen bonding. The HEMA-based system's carbonyl band shifted from 1682.38 cm^{-1} to 1679.12 cm^{-1}, while the HEA-based film showed a similar shift from 1681.87 cm^{-1} to 1678.34 cm^{-1}. The HPMA-based film exhibited a smaller shift from 1682.82 cm^{-1} to 1681.66 cm^{-1}.

Minimal changes were observed in the Amide II region, which relates to N—H bending and C—N stretching, for the HEMA- and HPMA-based systems. In these, the band shifted slightly or remained nearly unchanged, suggesting that urethane linkages were largely preserved. Specifically, the band in the HEMA-based sample shifted from 1530.16 cm^{-1} to 1528.44 cm^{-1}, while in the HPMA-based film it remained stable (1529.21 cm^{-1} to 1529.45 cm^{-1}). However, a new band at 1536.38 cm^{-1} appeared in the HEA-based PUA after sol–gel treatment, indicating localized structural rearrangements, possibly due to enhanced urea-type hydrogen bonding or changes in the C—N bonding environment caused by interaction with the siloxane network.

Further evidence of structural reorganization was seen in the C—N stretching region. In the HEMA-based PUA, a notable band shift from 1355.77 cm^{-1} to 1334.52 cm^{-1} suggested modifications in the urethane environment. New bands emerged at 1335.37 cm^{-1} and 1335.87 cm^{-1} in the HEA- and HPMA-based systems, respectively, indicating stronger interactions between the organic matrix and the siloxane phase.

In the fingerprint region, additional signs of siloxane incorporation were detected. In the HPMA-based system, a strong shift from 1170.00 cm^{-1} to 1040.33 cm^{-1} and a new band at 1128.72 cm^{-1} indicated the formation of Si–O–C and Si–O–Si bonds. The HEA-based formulation similarly showed new bands at 1130.40 cm^{-1} and 1335.37 cm^{-1}, supporting the presence of well-organized siloxane domains.

FTIR spectroscopy was employed to confirm chemical changes in the SHPUA networks before and after sol–gel modification. As shown in Fig. 1, after UV curing and sol–gel reaction, all systems exhibited the appearance of strong absorption bands between 1040 and 1130 cm^{-1}, corresponding to Si–O–Si asymmetric stretching vibrations, indicative of network formation via siloxane condensation. Simultaneously, the Si–OH band near 950–960 cm^{-1} was reduced but not completely eliminated, suggesting incomplete condensation of alkoxysilane groups.

This observation aligns with the intentionally limited hydrolysis strategy (H_2O/Si–OEt = 1) employed during synthesis. Previous work by Xu et al. [26] confirmed via ^{29}Si NMR that under similar low-water, weak-acid conditions, silane species remain partially condensed (T_1–T_2 dominant), preserving some residual ethoxy or silanol groups. Our FTIR results are therefore consistent with a partially condensed hybrid network, where the formation of Si–O–Si domains improves thermal and mechanical properties, but complete inorganic network conversion is deliberately avoided to maintain processability and film integrity.

3.2. Deconvolution of the carbonyl (C=O) region

To better understand the hydrogen bonding environment and crosslinking behavior in the polyurethane acrylate (PUA) systems, the carbonyl stretching region (1800–1600 cm^{-1}) of the HEMA-, HEA-, and HPMA-based HPUA films—both before and after sol–gel modification—was analyzed using FTIR spectroscopy. Gaussian curve-fitting was used to separate overlapping peaks and identify individual contributions from free urethane carbonyl groups, mono-dentate hydrogen-bonded urea, and bidentate urea species (Tables 2, 3). The detailed deconvoluted spectra can be found in the supplementary material (Figs. S1–S6).

Before sol–gel treatment, the FTIR spectra of the HEMA- and HPMA-based HPUA films showed two distinct absorption bands. A smaller peak near 1725 cm^{-1} corresponded to free urethane carbonyls, while a stronger band between 1681 and 1682 cm^{-1} was attributed to mono-dentate hydrogen-bonded urea groups. These bands are characteristic of urea linkages derived from the biuret structure of hexamethylene diisocyanate. In the HEMA-based film, the free urethane carbonyl appeared at 1725.01 cm^{-1} (area = 2.63), and the dominant mono-dentate urea band at 1682.19 cm^{-1} (area = 11.60). A similar pattern was observed for the HPMA-based formulation, with peaks at 1724.76 cm^{-1} (area = 2.10) and 1681.52 cm^{-1} (area = 11.78). The HEA-based HPUA showed a broader, less defined band centered at 1680.13 cm^{-1} (area = 5.05) and a shoulder around 1726.12 cm^{-1}, suggesting a dominant presence of mono-dentate urea species and a lower amount of free urethane groups.

After sol–gel modification, the carbonyl region became more complex, indicating stronger hydrogen bonding and enhanced interaction between the polymer matrix and the developing inorganic siloxane network. In the HEMA-based SHPUA, the free urethane carbonyl band decreased in intensity and shifted to 1719.59 cm^{-1} (area = 2.21), while the mono-dentate urea band at 1679.79 cm^{-1} remained prominent (area = 9.09). Notably, a new peak appeared at 1643.07 cm^{-1} (area = 1.78), attributed to bidentate hydrogen-bonded urea species. This new band points to stronger intermolecular interactions and greater crosslinking, likely due to reactions between urea functionalities and siloxane groups formed during the sol–gel process.

The HEA-based SHPUA showed a dominant mono-dentate urea band at 1679.69 cm^{-1} (area = 14.38), with a faint shoulder at 1726.38 cm^{-1} indicating residual free urethane content. Similarly, the HPMA-based SHPUA exhibited a weak free urethane peak at 1726.34 cm^{-1} (area = 0.94) and a strong mono-dentate urea band at 1680.43 cm^{-1} (area = 8.11). These spectral changes confirm that sol–gel treatment enhances hydrogen bonding and network density, with the degree of crosslinking and urea interaction varying depending on the type of acrylate monomer used.

Table 2
Deconvolution data of C═O stretching bands for HPUA polymers, obtained using Gaussian fitting analysis.

Sample designation	Free urethane		H-bonded urethane		Mono-dentate H-bonded urea		Bidentate H-bonded urea	
	cm^{-1}	Area	cm^{-1}	Area	cm^{-1}	Area	cm^{-1}	Area
HEMA-HPUA	1725.01	2.63	–	–	1682.19	11.60	–	–
HEA-HPUA	1726.12(sh)[a]	–	–	–	1680.13	5.05	–	–
HPMA-HPUA	1724.76	2.10	–	–	1681.52	11.78	–	–

[a] sh = shoulder.

Table 3
Deconvolution data of C═O stretching bands for SHPUA polymers, obtained using Gaussian fitting analysis.

Sample designation	Free urethane		H-bonded urethane		Mono-dentate H-bonded urea		Bidentate H-bonded urea	
	cm^{-1}	Area	cm^{-1}	Area	cm^{-1}	Area	cm^{-1}	Area
HEMA-SHPUA	–	–	1719.59	2.21	1679.79	9.09	1643.07	1.78
HEA-SHPUA	1723.38(sh)[a]	–	–	–	1679.69	14.38	–	–
HPMA-SHPUA	1726.34	0.94	–	–	1680.43	8.11	–	–

[a] sh = shoulder.

3.3. DSC and gel content analysis

DSC was employed to evaluate the thermal transitions of HPUA films before and after sol–gel modification. Across all formulations, a notable increase in T_g was observed following sol–gel treatment, indicating that the formation of silica-based inorganic networks effectively restricted polymer chain mobility and increased the overall network rigidity. The corresponding DSC thermograms are provided in the Supplementary Information (Figs. S7–S8).

For the HEMA-based HPUA, T_g increased from 5.16 °C to 27.55 °C, reflecting moderate improvement in crosslinking density and reasonable compatibility between the polymer matrix and the siloxane domains (Tables 4 and 5). In the HEA-based formulation, a smaller T_g shift from −9.37 °C to −2.84 °C was observed, suggesting limited interfacial bonding with the inorganic network and lower crosslinking efficiency. In contrast, the HPMA-based system exhibited a dramatic T_g rise from −13.52 °C to 90.0 °C after sol–gel modification, implying substantial restriction of chain motion and suggesting strong interaction with the inorganic phase [27,28].

To further validate the crosslinking behavior, gel content measurements were conducted via extraction method using acetone. The results are presented in Tables 4 and 5. While the HEMA-based SHPUA achieved complete curing with a gel content of 100 %, the HEA- and HPMA-based systems reached 92.19 % and 89.03 %, respectively. Notably, despite exhibiting the highest T_g, the HPMA-based film did not show the highest gel content.

This apparent discrepancy suggests that T_g alone is not a definitive indicator of crosslink density. In the case of HPMA–SHPUA, the high T_g may result from segmental rigidity imposed by the hydroxypropyl side groups and vitrification during curing, which restricts molecular mobility and prematurely halts double bond conversion. This behavior is consistent with previous reports, where vitrification effects limited the extent of polymerization in UV-curable acrylate systems [29,30].

Thus, gel content and T_g provide complementary but distinct information: while T_g reflects the thermomechanical state of the polymer, gel content offers a direct measure of network formation and chemical crosslinking. In HPMA–SHPUA, the moderate gel content (89.03 %) indicates an incomplete, yet highly rigid network, highlighting the complex interplay between chemical and physical factors during UV curing.

Table 4
T_g and Gel content of HPUA films.

Sample designation	Monomer type	T_g (°C)	Gel content (wt%)
HEMA-HPUA	HEMA	5.16	92.45
HEA-HPUA	HEA	−9.37	89.01
HPMA-HPUA	HPMA	−13.52	82.14

Table 5
T_g and Gel content of SHPUA films.

Sample designation	Monomer type	T_g (°C)	Gel content (wt%)
HEMA-SHPUA	HEMA	27.55	100
HEA-SHPUA	HEA	−2.84	92.19
HPMA-SHPUA	HPMA	90.0	89.03

3.4. TGA analysis

The thermal stability of the HPUA and sol–gel-modified SHPUA films was evaluated using TGA under a nitrogen atmosphere. The corresponding thermograms are provided in the supplementary material (Figs. S9–S10). All samples exhibited a typical three-stage thermal degradation profile. The first stage, occurring between 25 and 250 °C, was attributed to the evaporation of residual moisture, unreacted monomers, and low-molecular-weight oligomers. The second stage, observed between 250 and 350 °C, corresponded to the breakdown of urethane linkages, resulting in the release of degradation products such as amines, isocyanates, alcohols, and carbon dioxide. The third stage, taking place above 400 °C, involved the decomposition of the main polyurethane backbone [31].

After sol–gel treatment, all formulations showed notable improvements in thermal stability. This enhancement is attributed to the in situ formation of silica domains within the polymer matrix, which act as thermal barriers that slow down heat transfer and thermal degradation.

For the HEMA-based system, the temperature at which 10 % weight loss occurred (T_{10}) increased from 219 °C to 299 °C, while the temperature at 50 % weight loss (T_{50}) increased from 418 °C to 447 °C. The maximum degradation rate also decreased from 1.193 %/min to 0.63 %/min, indicating moderate thermal reinforcement through silica incorporation (Tables 6, 7).

In the HEA-based film, T_{10} rose significantly from 152 °C to 292 °C, and T_{50} increased from 384 °C to 446 °C. The maximum degradation rate dropped sharply from 2.82 %/min to 0.62 %/min. These improvements suggest effective interaction between the HEA monomer and the forming siloxane network, possibly aided by the flexible ethyl side chain, which may facilitate better integration with the inorganic phase.

The HPMA-based HPUA also demonstrated substantial thermal stabilization after sol–gel modification. T_{10} increased from 159 °C to 237 °C, while T_{50} rose markedly from 380 °C to 457 °C. The maximum degradation rate decreased from 2.28 %/min to 0.92 %/min. These

Table 6
Effect of acrylic monomer type on the thermal properties of HPUA.

HPUA	Thermal degradation step	T_{max} /°C	T_{onset} /°C	T_{endset} /°C	$(dw/dt)_{max}$ (% min^{-1})	$T_{10\%}$ /°C	$T_{50\%}$ /°C
HEMA-	I	223	77	287	1.19	219	418
	II	344	287	390	7.27		
	III	462	390	565	9.34		
HEA-	I	155	69	268	2.82	152	384
	II	350	268	409	4.12		
	III	442	409	524	90.22		
HPMA-	I	169	43	279	2.28	159	380
	II	340	279	392	5.45		
	III	463	392	587	6.46		

Table 7
Effect of acrylic monomer type on the thermal properties of SHPUA.

SHPUA	Thermal degradation step	T_{max} /°C	T_{onset} /°C	T_{endset} /°C	$(dw/dt)_{max}$ (% min^{-1})	$T_{10\%}$ /°C	$T_{50\%}$ /°C
HEMA-	I	174	83	250	0.63	299	447
	II	345	270	385	3.27		
	III	463	395	545	10.92		
HEA-	I	170	73	238	0.62	292	446
	II	344	255	380	5.33		
	III	470	394	606	10.19		
HPMA-	I	180	89	263	0.92	237	457
	II	342	289	390	9.34		
	III	445	404	538	29.10		

results confirm the formation of a well-developed silica network that significantly enhances thermal resistance. The strong compatibility between the HPMA structure and the siloxane phase likely promotes hydrogen bonding and condensation reactions during the sol–gel process, leading to the formation of a more robust and highly crosslinked hybrid structure.

3.5. Gloss and contact angle studies

The surface properties of the HPUA films were evaluated using water contact angle and gloss measurements to understand how sol–gel processing and acrylate monomer structure affect hydrophobicity and optical appearance.

3.5.1. Contact angle measurements

All HPUA films showed a clear increase in water contact angle after sol–gel modification, indicating improved surface hydrophobicity. This enhancement is mainly due to the formation of hydrophobic siloxane (Si–O–Si) linkages, generated through the hydrolysis and condensation of MPTMS. These linkages lower the surface polarity of the cured films, leading to greater water repellency. As summarized in Tables 8 and 9, the contact angle for the HEMA-based polymer increased from 100° to 130°, while the HEA-based and HPMA-based systems increased from 75° to 106° and from 83° to 105°, respectively.

Among the three, the HEMA-based formulation showed the largest increase in contact angle, suggesting more effective surface migration and alignment of silane species. The HEA-based film, which initially had the lowest contact angle, also showed a substantial improvement, confirming that the sol–gel network enhances hydrophobicity even in relatively hydrophilic systems. The HPMA-based system, which was already more hydrophobic due to its branched side chains, displayed a more modest increase, indicating that the sol–gel effect on surface energy was less pronounced in this formulation.

Table 8
Gloss values and water contact angle measurements of HPUA films.

HPUA	Gloss (°)			Contact angle (°)
	20	60	85	
HEMA-	66	122	86	100
HEA-	78	94	82	75
HPMA-	63	95	87	83

Table 9
Gloss values and water contact angle measurements of SHPUA.

SHPUA	Gloss (°)			Contact angle (°)
	20	60	85	
HEMA-	78	133	92	130
HEA-	80	106	89	106
HPMA-	78	98	95	105

3.5.2. Gloss measurements

Gloss values were measured at 20°, 60°, and 85° incident angles to assess surface reflectivity and smoothness before and after sol–gel modification (Tables 8, 9). For the HEMA-based films, gloss increased at all angles—from 66°, 122°, and 86° to 78°, 133°, and 92°, respectively. This improvement suggests that the silica network was well-dispersed, leading to a smoother surface and enhanced specular reflection. In contrast, the HPMA-based films experienced a decrease in gloss, especially at 60°, where gloss dropped to 98°, the lowest among the formulations. This reduction points to a matting effect likely caused by increased surface roughness due to phase separation or incomplete siloxane dispersion.

The HEMA-based system, with its better compatibility with the siloxane phase, resulted in more uniform surface morphology and higher gloss values. The HEA-based films showed intermediate behavior, with relatively small changes in gloss across all angles. This suggests a moderate balance between silica dispersion and surface heterogeneity, maintaining relatively consistent optical performance.

3.6. Hardness tests

The condensation of silanol groups during the sol–gel process led to the formation of a compact inorganic silica network within the polymer matrix, contributing to improved mechanical performance. This reinforcement effect was evident in the pencil hardness test results, where all HPUA formulations showed increased surface hardness after sol–gel modification.

In both the HEMA- and HPMA-based films, pencil hardness increased from F to H, indicating that the incorporation of the silica phase enhanced the resistance of the surface to mechanical deformation. The HEMA-based system, in particular, benefited from improved interfacial bonding between the polymer and the inorganic domains, resulting in a noticeable increase in surface hardness (Table 10).

The HEA-based formulation showed the most significant relative improvement in hardness, rising from 2B to H. This substantial gain is attributed to the initially lower mechanical strength of the HEA-based film, which stems from the flexible ethyl side chain structure. The sol–gel process effectively compensated for this softness by reinforcing the network through silica incorporation.

The HPMA-based film, characterized by its bulky and hydrophobic

Table 10
Pencil hardness values of HPUA and SHPUA films.

Sample	HPUA	SHPUA
HEMA-	F	H
HEA-	2B	H
HPMA-	F	H

side chain, also exhibited a hardness increase from F to H. Although its initial mechanical strength was higher due to steric hindrance from the HPMA structure, the overall improvement in hardness was more modest. This suggests that the pre-existing rigidity of the HPMA-based system may limit the extent of mechanical enhancement achievable through sol–gel modification.

3.7. SEM analysis of HPUA films

To evaluate the internal cohesion, structural integrity, and surface quality of the cured films, cross-sectional and surface SEM images were obtained for all HPUA formulations (Fig. 2). These micrographs provide insight into the influence of acrylate monomer structure on film morphology, network formation, and mechanical failure modes.

The HEMA-based HPUA film exhibited a dense and glassy cross-section with minimal porosity and clean, planar fracture surfaces. The morphology suggests a brittle fracture mechanism typical of highly crosslinked, cohesive thermosets. Surface SEM revealed a smooth, defect-free morphology without any visible phase separation, cracks, or micropores. These features align with the relatively high gel content (92.45 %), moderate T_g (5.16 °C), and high optical gloss, confirming that HEMA contributes to uniform network formation and excellent surface curing characteristics.

In contrast, the HEA-based HPUA film showed a loosely packed lamellar structure in cross-section with slightly undulated fracture paths and intermittent voids. The fracture behavior indicated a semi-ductile response, likely due to the flexible ethylene side chains of HEA that reduce segmental packing and hydrogen bonding. Surface SEM revealed subtle ridges and surface undulations, reflecting partial surface shrinkage and lower cohesive energy. These findings are consistent with its lower T_g (−9.37 °C) and moderate gel content (89.01 %), suggesting an intermediate degree of crosslinking and less homogeneous polymerization near the surface.

The HPMA-based HPUA film displayed a distinctly heterogeneous cross-sectional morphology, characterized by rough fracture planes, microvoids, and an irregular texture. These features point to a mixed brittle–ductile fracture mechanism, resulting from interrupted phase continuity caused by the bulky hydroxypropyl groups of HPMA. The surface morphology exhibited granular textures, uneven topography, and localized microcracks—hallmarks of poor surface leveling and steric hindrance during curing. These features are consistent with the formulation's lowest gel content (82.14 %) and lowest T_g (−13.52 °C), indicating limited crosslink density and non-uniform network formation both internally and at the film–air interface.

Overall, SEM analysis demonstrates that monomer side chain architecture strongly governs both internal and surface morphology of HPUA films. HEMA-based systems form compact and smooth networks with brittle failure, HEA-based systems exhibit moderate flexibility with surface irregularities, while HPMA-based films suffer from steric disruption, reduced crosslinking, and compromised structural homogeneity.

4. Conclusions

This study presented the successful synthesis and dual chemical modification of hybrid polyurethane acrylate films using a pentaerythritol core, biuret-HDI as the isocyanate, and three acrylate monomers—HEMA, HEA, and HPMA. The films were further functionalized through thiol–ene click reactions and sol–gel processing via MPTMS incorporation. The effects of monomer structure on thermal, morphological, and surface properties were systematically investigated.

FTIR analysis confirmed the formation of Si–O–Si networks after sol–gel modification, evidenced by the appearance of a strong absorption band near 1130 cm^{-1}. This incorporation enhanced thermal stability and contributed to distinct microstructural differences across the formulations. Among them, the HPMA-based SHPUA film exhibited the highest increase in T_g (from −13.52 °C to 90.0 °C), superior hardness, and more rigid morphology. These enhancements are attributed to enhanced vitrification and steric effects that restricted chain mobility, despite a lower gel content.

The HEMA-based system demonstrated balanced performance with the highest gel content (100 %) and a smooth, uniform microstructure, indicating excellent compatibility with the siloxane network and efficient surface curing. It also showed improved T_g and strong chemical resistance, making it suitable for applications requiring cohesive, high-gloss coatings.

Importantly, while the HEA-based SHPUA system showed only modest gains in T_g and gel content, it achieved a substantial improvement in thermal stability, with a 140 °C increase in T_{10} temperature. FTIR spectra confirmed Si–O–Si network formation, indicating effective sol–gel integration. These results highlight that the HEA-based system, despite its flexible molecular structure, significantly benefited from

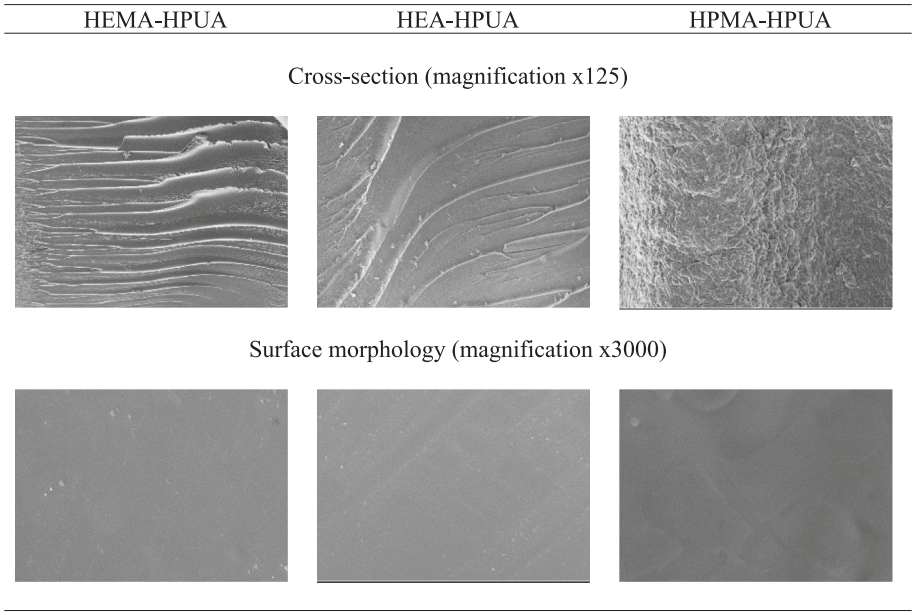

Fig. 2. SEM images of UV-cured HPUA films based on HEMA, HEA, and HPMA.

inorganic phase incorporation in terms of thermal performance.

Morphological analysis via SEM supported these findings. HEMA-based films exhibited dense and brittle fractures, HEA-based films showed semi-ductile and lamellar features, and HPMA-based systems revealed heterogeneous, rough textures associated with steric hindrance and interrupted phase continuity. The observed surface features correlated well with contact angle, gloss, and gel content data.

Overall, this work demonstrates that monomer architecture plays a decisive role in determining the degree and uniformity of network formation during sol–gel and thiol–ene modification. The study provides new insights into tailoring UV-curable hybrid coatings by selecting monomers based on desired balance of flexibility, crosslink density, and thermal performance.

CRediT authorship contribution statement

Bilge Eren: Writing – review & editing, Supervision, Project administration, Methodology. **Sibel Taşpınar:** Formal analysis. **Rabia Balcı:** Formal analysis. **Beyhan Erdoğan:** Formal analysis.

Declaration of competing interest

The authors declare that they have no known competing financial interests or personal relationships that could have appeared to influence the work reported in this paper.

Acknowledgments

This study was supported by Bilecik Şeyh Edebali University with the project number GAP-2024-590. The authors also thank DYO Paint Factories, Izmir, for the polymers' DSC analysis, contact angle, and gloss measurements.

Appendix A. Supplementary data

Supplementary data to this article can be found online at https://doi.org/10.1016/j.reactfunctpolym.2025.106452.

Data availability

No data was used for the research described in the article.

References

[1] R.P. Brannigan, A. Walder, A.P. Dove, Application of functional diols derived from pentaerythritol as chain extenders in the synthesis of novel thermoplastic polyester-urethane elastomers, Polym. Chem. 10 (2019) 5236–5241, https://doi.org/10.1039/C9PY00951E.

[2] W. Chen, C. Chen, W. Yan, C. Yi, S. Wu, K.W.K. Yeung, Z. Xu, Synthesis and characterization of novel highly branched block copoly(urethane-imide)s based on pentaerythritol, different diisocyanate and aromatic dianhydride, J. Appl. Polym. Sci. 118 (1) (2010) 99–104, https://doi.org/10.1002/app.32398.

[3] T.K. Cho, M.H. Chong, B.C. Chun, H.R. Kim, Y.C. Chung, Structure-property relationship and shape memory effect of polyurethane copolymer cross-linked with pentaerythritol, Fibers Polym. 8 (2007) 7–12, https://doi.org/10.1007/BF02908153.

[4] Y.C. Chung, T.K. Cho, B.C. Chun, Flexible cross-linking by both pentaerythritol and polyethyleneglycol spacer and its impact on the mechanical properties and the shape memory effects of polyurethane, J. Appl. Polym. Sci. 112 (2009) 2800–2808.

[5] B. Das, U. Konwar, M. Mandal, N. Karak, Sunflower oil based biodegradable hyperbranched polyurethane as a thin film material, Ind. Crop. Prod. 44 (2013) 396–404, https://doi.org/10.1016/j.indcrop.2012.11.028.

[6] S. Lu, T. Shen, J. Xing, Q. Song, J. Shao, J. Zhang, C. Xin, Preparation and characterization of cross-linked polyurethane shell microencapsulated phase change materials by interfacial polymerization, Mater. Lett. 211 (2018) 36–39, https://doi.org/10.1016/j.matlet.2017.09.074.

[7] A. Patel, C. Patel, M.G. Patel, M. Patel, A. Dighe, Fatty acid modified polyurethane dispersion for surface coatings: effect of fatty acid content and ionic content, Prog. Org. Coat. 67 (3) (2010) 255–263, https://doi.org/10.1016/j.porgcoat.2009.11.006.

[8] B. Tang, W. Feng, J. Guo, J. Sun, S. Zhang, X. Gu, H. Li, W. Yang, Hydrophobic modification of pentaerythritol and its application in fire-retardant coatings for steel structures, Prog. Org. Coat. 138 (2020) 105391, https://doi.org/10.1016/j.porgcoat.2019.105391.

[9] W. Shihai, Y. Zhou, B.A. Zhuang, P. Zheng, H. Chen, T. Zhang, H. Hu, D. Huang, Star-shaped amphiphilic block polyurethane with pentaerythritol core for a hydrophobic drug delivery carrier, Polym. Int. 65 (2016) 551–558, https://doi.org/10.1002/pi.5092.

[10] D. Wei, B. Liao, J. Huang, Z. Min, H. Pang, Fabrication of castor oil-based hyperbranched urethane acrylate UV-curable coatings via thiol-ene click reactions, Prog. Org. Coat. 135 (2019) 114–122, https://doi.org/10.1016/j.porgcoat.2019.05.039.

[11] S. Tasić, B. Božić, B. Dunjić, Synthesis of new hyperbranched urethane-acrylates and their evaluation in UV-curable coatings, Prog. Org. Coat. 51 (4) (2004) 320–327, https://doi.org/10.1016/j.porgcoat.2004.07.005.

[12] E. Džunuzović, S. Tasić, B. Božić, D. Babić, B. Dunjić, UV-curable hyperbranched urethane acrylate oligomers containing soybean fatty acids, Prog. Org. Coat. 52 (2) (2005) 136–143, https://doi.org/10.1016/j.porgcoat.2004.10.003.

[13] E.S. Džunuzović, S.V. Tasić, B.R. Božić, J.V. Džunuzović, B.M. Dunjić, K.B. Jeremić, Mechanical and thermal properties of UV cured mixtures of linear and hyperbranched urethane acrylates, Prog. Org. Coat. 74 (1) (2012) 158–164, https://doi.org/10.1016/j.porgcoat.2011.12.004.

[14] Q. Zhang, C. Huang, H. Wang, M. Hu, H. Li, X. Liu, UV-curable coating crosslinked by a novel hyperbranched polyurethane acrylate with excellent mechanical properties and hardness, RSC Adv. 6 (109) (2016) 107318–107324, https://doi.org/10.1039/C6RA21081C.

[15] J. Fu, H. Yu, L. Wang, L. Lin, R.U. Khan, Preparation and properties of UV-curable hyperbranched polyurethane acrylate hard coatings, Prog. Org. Coat. 144 (2020) 105635, https://doi.org/10.1016/j.porgcoat.2020.105635.

[16] G. Xu, W. Shi, Synthesis and characterization of hyperbranched polyurethane acrylates used as UV curable oligomers for coatings, Prog. Org. Coat. 52 (2) (2005) 110–117, https://doi.org/10.1016/j.porgcoat.2004.10.002.

[17] H. Xiang, X. Wang, G. Lin, L. Xi, Y. Yang, D. Lei, H. Dong, J. Su, Y. Cui, X. Liu, Preparation, characterization, and application of UV-curable flexible hyperbranched polyurethane acrylate, Polymers (Basel) 9 (11) (2017) 552, https://doi.org/10.3390/polym9110552.

[18] H. Hu, Y. Yuan, W. Shi, Preparation of waterborne hyperbranched polyurethane acrylate/LDH nanocomposite, Prog. Org. Coat. 75 (4) (2012) 474–479, https://doi.org/10.1016/j.porgcoat.2012.06.007.

[19] W. Han, B. Lin, H. Yang, X. Zhang, Synthesis and properties of UV-curable hyperbranched polyurethane acrylate oligomers containing carboxyl groups, Polym. Bull. 68 (2012) 1009–1022, https://doi.org/10.1007/s00289-011-0597-6.

[20] X. Jiao, J. Liu, J. Jin, F. Cheng, Y. Fan, L. Zhang, G. Lai, X. Hua, X. Yang, UV-cured transparent silicone materials with high tensile strength prepared from hyperbranched silicon-containing polymers and polyurethane-acrylates, ACS Omega 6 (4) (2021) 2890–2898, https://doi.org/10.1021/acsomega.0c05243.

[21] P. Alagi, Y.J. Choi, J. Seog, S.C. Hong, Efficient and quantitative chemical transformation of vegetable oils to polyols through a thiol-ene reaction for thermoplastic polyurethanes, Ind. Crop. Prod. 87 (2016) 78–88, https://doi.org/10.1016/j.indcrop.2016.04.027.

[22] J. Bai, H. Li, Z. Shi, J. Yin, An eco-friendly scheme for the cross-linked polybutadiene elastomer via thiol–ene and Diels–Alder click chemistry, Macromolecules 48 (11) (2015) 3539–3546, https://doi.org/10.1021/acs.macromol.5b00389.

[23] Y. Cao, Z. Liu, B. Zheng, R. Ou, Q. Fan, L. Li, C. Guo, T. Liu, Q. Wang, Synthesis of lignin-based polyols via thiol-ene chemistry for high-performance polyurethane anticorrosive coating, Compos. B Eng. 200 (2020) 108295, https://doi.org/10.1016/j.compositesb.2020.108295.

[24] X. Ding, X. Wang, H. Zhang, T. Liu, C. Hong, Q. Ren, C. Zhou, Preparation of waterborne polyurethane-silica nanocomposites by a click chemistry method, Mater Today Commun 23 (2020) 100911, https://doi.org/10.1016/j.mtcomm.2020.100911.

[25] B. Liang, R. Li, C. Zhang, Z. Yang, T. Yuan, Synthesis and characterization of a novel tri-functional bio-based methacrylate prepolymer from castor oil and its application in UV-curable coatings, Ind. Crop. Prod. 135 (2019) 170–178, https://doi.org/10.1016/j.indcrop.2019.04.039.

[26] J. Xu, W. Pang, W. Shi, Synthesis of UV-curable organic–inorganic hybrid urethane acrylates and properties of cured films, Thin Solid Films 514 (1–2) (2006) 69–75, https://doi.org/10.1016/j.tsf.2006.02.032.

[27] B. Eren, E. Demir Karaçoban, B. Erdoğan, E. Eren, Effect of PEG molecular mass and HEMA capping on the thermal, morphological, and hydrophilic properties of isocyanate-terminated polyurethane acrylate films, J. Therm. Anal. Calorim. 148 (21) (2023) 11683–11694, https://doi.org/10.1007/s10973-023-12507-4.

[28] B. Eren, H. Çınar, B. Erdoğan, Effect of 2-hydroxyethyl methacrylate content on the emulsion polymerization process of styrene–butyl acrylate–acrylic acid: chemical, thermal and film properties of polymer latex, J. Therm. Anal. Calorim. 147 (23) (2022) 13289–13299, https://doi.org/10.1007/s10973-022-11559-2.

[29] X. Wang, M.D. Soucek, Investigation of non-isocyanate urethane dimethacrylate reactive diluents for UV-curable polyurethane coatings, Prog. Org. Coat. 76 (8) (2013) 1057–1067, https://doi.org/10.1016/j.porgcoat.2013.03.001.

[30] J.-S. Choi, J. Seo, S.B. Khan, E.S. Jang, H. Han, Effect of acrylic acid on the physical properties of UV-cured poly(urethane acrylate-co-acrylic acid) films for metal coating, Prog. Org. Coat. 71 (1) (2011) 110–116, https://doi.org/10.1016/j.porgcoat.2011.01.00.

[31] B. Eren, E.D. Karaçoban, B. Erdoğan, Synthesis and characterization of UV-curable polyurethane acrylates derived from trimethylolpropane and hydroxyethyl methacrylate: effect of 2-hydroxyethyl methacrylate (HEMA) content on thermal

stability, gloss properties, and microstructure, Polym. Eng. Sci. 65 (1) (2025) 327–337, https://doi.org/10.1002/pen.27012.